
Personalized Federated Learning with Gaussian Processes

Idan Achituve*
Bar-Ilan University, Israel

Aviv Shamsian
Bar-Ilan University, Israel

Aviv Navon
Bar-Ilan University, Israel

Gal Chechik
Bar-Ilan University, Israel
NVIDIA, Isreal

Ethan Fetaya
Bar-Ilan University, Israel

Abstract

Federated learning aims to learn a global model that performs well on client devices with limited cross-client communication. Personalized federated learning (PFL) further extends this setup to handle data heterogeneity between clients by learning personalized models. A key challenge in this setting is to learn effectively across clients even though each client has unique data that is often limited in size. Here we present *pFedGP*, a solution to PFL that is based on Gaussian processes (GPs) with deep kernel learning. GPs are highly expressive models that work well in the low data regime due to their Bayesian nature. However, applying GPs to PFL raises multiple challenges. Mainly, GPs performance depends heavily on access to a good kernel function, and learning a kernel requires a large training set. Therefore, we propose learning a shared kernel function across all clients, parameterized by a neural network, with a personal GP classifier for each client. We further extend pFedGP to include inducing points using two novel methods, the first helps to improve generalization in the low data regime and the second reduces the computational cost. We derive a PAC-Bayes generalization bound on novel clients and empirically show that it gives non-vacuous guarantees. Extensive experiments on standard PFL benchmarks with CIFAR-10, CIFAR-100, and CINIC-10, and on a new setup of learning under input noise show that pFedGP achieves well-calibrated predictions while significantly outperforming baseline methods, reaching up to 21% in accuracy gain.

1 Introduction

In recent years, there is a growing interest in applying learning in decentralized systems under the setup of federated learning (FL) [33, 47, 61]. In FL, a server node stores a global model and connects to multiple end-devices (“clients”), which have private data that cannot be shared. The goal is to learn the global model in a communication-efficient manner. However, learning a single shared model across all clients may perform poorly when the data distribution varies significantly across clients. *Personalized Federated Learning* (PFL) [62] addresses this challenge by jointly learning a personalized model for each client. While significant progress had been made in recent years, leading approaches still struggle in realistic scenarios. First, when the amount of data per client is limited, even though this is one of the original motivations behind federated learning [4, 47, 67]. Second, when the *input* distribution shifts between clients, which is often the case, as clients use different devices and sensors. Last, when we require well-calibrated predictions, which is an important demand from medical and other safety-critical applications.

*Correspondence to: Idan Achituve <Idan.Achituve@biu.ac.il>

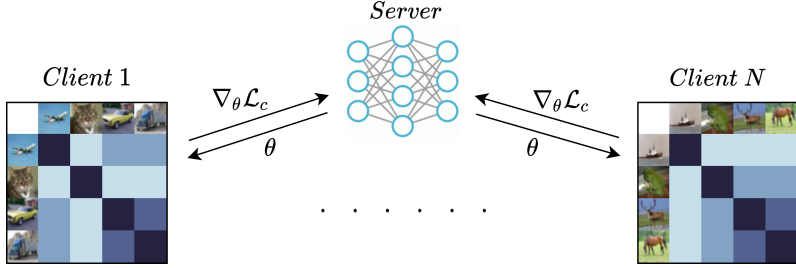


Figure 1: pFedGP - learning a shared deep kernel function with client-specific GP models. Each client stores private data, possibly from a different distribution. The data is first mapped to an embedding space with a shared neural network across all clients. Then, using common kernels a GP is applied to the data of the client for model learning and inference. We illustrate the per client kernel matrix $k_\theta(\mathbf{x}_i, \mathbf{x}_j)$. Bold cells indicate a stronger covariance.

Here, we show how *Gaussian Processes* (GPs) with deep kernel learning (DKL) [75] is an effective alternative for handling these challenges. GPs have good predictive performance in a wide range of dataset sizes [2, 76], they are robust to input noise [70], can adapt to shifts in the data distribution [44], and provide well-calibrated predictions [64]. While regression tasks are more natural for GPs, here we focus on classification tasks for consistency with common benchmarks and learning procedures in the field; however, our approach is also applicable to regression tasks.

Consider a naive approach that fits a separate GP classifier to each client based on its personal data. Its performance heavily depends on the quality of the kernel, and standard kernels tend to work poorly in domains such as images. A popular solution to this problem is to use deep kernel learning (DKL) [75], where a kernel is applied to features outputted by a neural network (NN). Unfortunately, GPs with DKL can strongly overfit, often even worse than standard NNs [52], and thus negate the main benefit of using a GP. We solve this issue by jointly learning a shared kernel function across clients. As the kernel captures similarities between inputs, a single kernel should work well across clients, while using a separate GP per client will give the required flexibility for personalization.

We adapt a GP classifier recently proposed in [2] which uses the Pólya-Gamma augmentation [53] in a tree-structure model to the federated setting. We term our method *pFedGP*. We extend pFedGP by tailoring two inducing point (IP) methods [54, 65]. The first helps generalization in the low data regime and, unlike common inducing point methods, does not reduce the computational costs. The second, does focus on reducing the computational cost to make our approach scalable and work in low-resource clients. We also adjust previous PAC-Bayes generalization bounds for GPs [56, 59] to include the Pólya-Gamma augmentation scheme. These bounds are suitable for cases where the kernel is not learned, such as when new clients arrive after the shared NN was already learned.

Therefore, this paper makes the following contributions: (i) introduce pFedGP as a natural solution to PFL; (ii) develop two IP methods to enhance GP classifiers that use the Pólya-Gamma augmentation scheme and integrate them with pFedGP; (iii) derive a PAC-Bayes generalization bound on novel clients and show empirically that it gives meaningful guarantees; (iv) achieve state-of-the-art results in a wide array of experiments, improving accuracy by up to 21%².

2 Related work

Federated learning. In FL, clients collaboratively solve a learning task while preserving data privacy and maintaining communication efficiency [1, 30, 38, 47, 50, 77, 80]. FedAvg [47] is an early but effective FL approach that updates models locally and averages them into a global model. Several optimization methods have been proposed for improving convergence in FL [37, 41, 66, 72]. Other approaches focus on preserving client privacy [3, 18, 48, 85], improving robustness to statistical diversity [24, 25, 28, 31, 82, 83], and reducing communication cost [12, 57]. These methods aim to learn a global model across clients, limiting their ability to deal with heterogeneous datasets.

²Our code is publicly available at <https://github.com/IdanAchituv/pFedGP>

Personalized federated learning. To overcome client heterogeneity, PFL aims to introduce some personalization for each client in the federation [35, 68]. Recent methods include adapting multitask learning [16, 62], meta-learning approaches [6, 19, 20, 39, 84], and model mixing, where clients learn a mixture of the global and local models [4, 15, 25, 40]. Other approaches utilize different regularization schemes to enforce soft parameter sharing [29, 67]. Personalization in FL has also been explored through clustering approaches in which similar clients within the federation have a greater effect on one another [45, 81]. Recently, [60] proposed learning a central hypernetworks that acts on client representation vectors for generating personalized models.

Bayesian FL. Some studies put forward a Bayesian treatment to the FL setup. [8, 11] used variational inference with Bayesian NNs. [71, 79] proposed a matching algorithm between local models based on the Beta-Bernoulli process to construct a global model. [78] proposed a FL framework that uses a global GP model for regression tasks and without DKL. Unlike this study, we focus on classification tasks with a personal GP classifier per client and advocate sharing information between clients through the kernel. [69] used GPs in a client selection strategy. In [32] an approach based on stein-variational gradient descent was suggested. This method does not scale beyond small-sized networks. [43] proposed a multivariate Gaussian product mechanism to aggregate local models. As we will show, this method is less suited when the data heterogeneity between clients is large.

Gaussian process classification. Unlike regression, in classification approximations must be used since the likelihood is not a Gaussian [55]. Classic approaches include the Laplace approximation [74], expectation-propagation [49], and least squares [58]. Recently, several methods were proposed based on the Pólya-Gamma augmentation [53] for modeling multinomial distributions [42], GP classification [21, 22, 73], few-shot learning [64], and incremental learning [2]. Here we build on the last approach. Classification with GPs is commonly done with variational inference techniques [27], here we wish to exploit the conjugacy of the model to take Gibbs samples from the posterior. This approach yields well calibrated [64] and more accurate models [2].

3 Gaussian processes background

We first provide a brief introduction to Gaussian Processes (GPs). Detailed explanations are deferred to the Appendix. We denote scalars with lower-case letters (e.g., x), vectors with bold lower-case letters (e.g., \mathbf{x}), and matrices with bold capital letters (e.g., \mathbf{X}). In general, $\mathbf{y} = [y_1, \dots, y_N]^T$ denotes the vector of labels, and $\mathbf{X} \in \mathbb{R}^{N \times d}$ the design matrix with N data points whose i^{th} row is \mathbf{x}_i .

Gaussian processes. GPs map input points to target output values via a random latent function f . f is assumed to follow a Gaussian process prior $f \sim \mathcal{GP}(m(\mathbf{x}), k(\mathbf{x}, \mathbf{x}'))$, where the evaluation vector of f on \mathbf{X} , $\mathbf{f} = [f(\mathbf{x}_1), \dots, f(\mathbf{x}_N)]^T$, has a Gaussian distribution $\mathbf{f} \sim \mathcal{N}(\boldsymbol{\mu}, \mathbf{K})$ with means $\boldsymbol{\mu}_i = m(\mathbf{x}_i)$ and covariance $K_{ij} = k(\mathbf{x}_i, \mathbf{x}_j)$. The mean $m(\mathbf{x})$ is often set to be the constant zero function, and the kernel $k(\mathbf{x}, \mathbf{x}')$ is a positive semi-definite function. The target values are assumed to be independent when conditioned on \mathbf{f} . For Gaussian process regression the likelihood is Gaussian, $p(\mathbf{y}|f) = \mathcal{N}(f, \sigma^2)$. Therefore, the posterior $p(f|\mathbf{y}, \mathbf{X})$ is also Gaussian, and both the marginal and the predictive distributions have known analytic expressions. This is one of the main motivations behind using GPs, as most other Bayesian models have intractable inference.

Unfortunately, for Gaussian process classification (GPC) the likelihood, $p(\mathbf{y}|f)$, is not a Gaussian and the posterior does not admit a closed-form expression. One approach for applying GPs to binary classification tasks is the Pólya-Gamma augmentation [53]. Using this approach, we can augment the GP model with random variables $\boldsymbol{\omega}$ from a Pólya-Gamma distribution, one for each example. As a result, $p(\mathbf{f}|\mathbf{y}, \mathbf{X}, \boldsymbol{\omega})$ is a Gaussian density and $p(\boldsymbol{\omega}|\mathbf{y}, \mathbf{X}, \mathbf{f})$ is a Pólya-Gamma density, both with known parameters. This allows us to use Gibbs sampling to efficiently sample from the posterior $p(\mathbf{f}, \boldsymbol{\omega}|\mathbf{y}, \mathbf{X})$ for inference and prediction. Full equations and further details on the Pólya-Gamma augmentation scheme are given in Appendix A.1.

Deep kernel learning (DKL). The quality of the GP model heavily depends on the kernel function $k(\mathbf{x}_i, \mathbf{x}_j)$. For many data modalities, such as images, common kernels are not a good measure of semantic similarity. Therefore, in [9, 75] it was suggested to use a standard kernel over features outputted by a NN. For example, the RBF kernel $k_\theta(\mathbf{x}_i, \mathbf{x}_j) = \exp\left(-\frac{\|\mathbf{g}_\theta(\mathbf{x}_i) - \mathbf{g}_\theta(\mathbf{x}_j)\|^2}{2\ell^2}\right)$. In regression, it is possible to directly backpropagate through the GP inference as it is given in closed-form. In our case, we can use Fisher’s identity [17] to obtain stochastic gradients of the kernel [64].

Inducing points. GPs require storing and inverting a kernel matrix on the entire training set which often limit its usage. A common solution to this problem is to use inducing point methods [54, 65]. The key idea is to replace the exact kernel by an approximation for fast computation. Usually we learn $M \ll N$ pseudo-inputs such that we need to invert an $M \times M$ matrix only.

GP-Tree. We build on GP-Tree [2], a recent GP classifier that was shown to scale well with dataset size and the number of classes. GP-Tree turns the multi-class classification problem into a sequence of binary decisions along the tree nodes. Each node in the tree fits a binary GP classifier based on the Pólya-Gamma augmentation scheme and the data associated with that node. The tree is constructed by first computing a prototype for each class and then recursively performing divisive hierarchical clustering on these prototypes to two clusters at each node. While GP-Tree outperformed other leading GPC methods in problems with many classes, we note that it may still struggle when the number of classes is extremely large. In such cases, this limitation will be reflected in our model as well. Further details on this method are given in Appendix A.2.

4 pFedGP: federated learning with Gaussian processes

Now we describe our approach for applying personalized federated learning (PFL) with Gaussian processes. First, we extend GP-Tree to the FL setup and show how to use Gibbs sampling to learn the NN parameters. Then, we present two alternatives for this method that use inducing points. The first is for extremely limited-size datasets, while the second allows controlling the computational resources. We name our method *pFedGP*. An illustration of our method is given in Figure 1.

4.1 A full GP model

The training procedure follows the standard protocol in this field [4, 40, 47]. We assume the existence of a server that holds the shared parameters (a NN). Let C denote the set of clients. For each client $c \in C$ we denote by D_c its local dataset of size N_c . At each training iteration the model is sent to $S \subseteq \{1, \dots, |C|\}$ clients to perform kernel learning. Each client $c \in S$ updates its copy of the global model and then sends the updated model to the server. The server then averages over the updates to obtain a new global model.

At each client c , we perform kernel learning in the following manner. We first compute the feature representation of the data samples associated with the client using the shared network. Then, we build the hierarchical classification tree as discussed in Section 3 & Appendix A.2. In [2] the tree was built only once after a pre-training stage and the model parameters were learned using a variational inference approach. Here, we re-build the tree at each round using the most recent features and we use a Gibbs sampling procedure, as it allows this flexibility in building the tree and performs better when not prohibitive by computational limitations. Learning the network parameters θ with the Gibbs sampling approach can be done with two common objectives, the marginal likelihood and the predictive likelihood.

We denote by \mathbf{X}_v the data associated with the tree node v , i.e., the data points which have v on the path from the root node to their class leaf node. We denote by \mathbf{y}_v the binary label of these points, i.e., does their path go left or right at this node. And we denote by ω_v the Pólya-Gamma random variables associated with node v . The marginal likelihood term for the full hierarchical classification tree is the sum of the separate marginal likelihood terms of all the nodes v in the tree:

$$\mathcal{L}_c^{ML}(\theta; D_c) = \sum_v \log p_\theta(\mathbf{y}_v | \mathbf{X}_v) = \sum_v \log \int p_\theta(\mathbf{y}_v | \omega_v, \mathbf{X}_v) p(\omega_v) d\omega_v. \quad (1)$$

Similar to [64] we use an approximate-gradient estimator based on Fisher's identity [17]:

$$\nabla_\theta \mathcal{L}_c^{ML}(\theta; D_c) = \sum_v \int p_\theta(\omega_v | \mathbf{y}_v, \mathbf{X}_v) \nabla_\theta \log p_\theta(\mathbf{y}_v | \omega_v, \mathbf{X}_v) d\omega_v \approx \sum_v \frac{1}{L} \sum_{l=1}^L \nabla_\theta \log p_\theta(\mathbf{y}_v | \omega_v^{(l)}, \mathbf{X}_v). \quad (2)$$

Here, $\omega_v^{(1)}, \dots, \omega_v^{(L)}$ are samples from the posterior at node v . Due to the Pólya-Gamma augmentation $p_\theta(\mathbf{y}_v | \omega_v^{(l)}, \mathbf{X}_v)$ is proportional to a Gaussian density. The exact expression is give in Appendix A.2.

To use the predictive likelihood as an objective, in each training iteration, after building the tree model, at each node we randomly draw a portion from the (node) training data and use it to predict

the class label for the remaining part. We denote with \mathbf{X}_v and \mathbf{y}_v the training portion, \mathbf{x}_v^* and y_v^* the input and the label of the point we are predicting, and P^{y^*} the path from the root node to the y^* leaf node (i.e., the original class). Here we also take advantage of the independence between nodes to maximize the likelihood per node individually. The predictive likelihood for a single data point:

$$\mathcal{L}_c^{PL}(\theta; \mathbf{x}^*, y^*) = \sum_{v \in P^{y^*}} \log p_\theta(y_v^* | \mathbf{x}_v^*, \mathbf{y}_v, \mathbf{X}_v) = \sum_{v \in P^{y^*}} \log \int p_\theta(y_v^* | \boldsymbol{\omega}_v, \mathbf{x}_v^*, \mathbf{y}_v, \mathbf{X}_v) p(\boldsymbol{\omega}_v) d\boldsymbol{\omega}_v. \quad (3)$$

Here, as well, we use an approximate-gradient estimator based on posterior samples of $\boldsymbol{\omega}$:

$$\nabla_\theta \mathcal{L}_c^{PL}(\theta; \mathbf{x}^*, y^*) \approx \sum_{v \in P^{y^*}} \frac{1}{L} \sum_{l=1}^L \nabla_\theta \log p_\theta(y_v^* | \boldsymbol{\omega}_v^{(l)}, \mathbf{x}_v^*, \mathbf{y}_v, \mathbf{X}_v). \quad (4)$$

Where $p_\theta(y_v^* | \boldsymbol{\omega}_v^{(l)}, \mathbf{x}_v^*, \mathbf{y}_v, \mathbf{X}_v) = \int p(y_v^* | f^*) p_\theta(f^* | \boldsymbol{\omega}_v^{(l)}, \mathbf{x}_v^*, \mathbf{y}_v, \mathbf{X}_v) df^*$ does not have an analytical expression, but $p_\theta(f^* | \boldsymbol{\omega}_v^{(l)}, \mathbf{x}_v^*, \mathbf{y}_v, \mathbf{X}_v) = \int p_\theta(f^* | \mathbf{f}, \mathbf{x}_v^*, \mathbf{X}_v) p_\theta(\mathbf{f} | \boldsymbol{\omega}_v^{(l)}, \mathbf{y}_v, \mathbf{X}_v) df^*$ is Gaussian with known parameters. We then compute the predictive likelihood by performing Gauss-Hermite integration over f^* . See exact expression in Appendix A.2.

4.2 Augmenting the model with inducing points: sample efficiency

The GP model described in Section 4.1 works well in most situations. However, when the number of data points per client is small, performance naturally degrades. To increase information sharing between clients and improve the per-client performance, we suggest augmenting the model with global inducing points shared across clients. When sending the model from the server to a client, we also send the inducing inputs and their labels. To streamline optimization and reduce the communication burden, we define the inducing inputs in the feature space of the last embedding layer of the shared NN. Therefore, usually, their size will be negligible compared to the network size.

We denote by $\bar{\mathbf{X}}$ the learned inducing inputs and by $\bar{\mathbf{y}}$ their fixed class labels. They are set evenly across classes. During training, we regard *only* the set of inducing inputs-labels $(\bar{\mathbf{X}}, \bar{\mathbf{y}})$ as the available (training) data and use them for posterior inference. More formally, we compute $p_\theta(\mathbf{f} | \bar{\boldsymbol{\omega}}, \bar{\mathbf{y}}, \bar{\mathbf{X}}, \mathbf{X}) = \int p_\theta(\mathbf{f} | \mathbf{f}, \bar{\mathbf{X}}, \mathbf{X}) p_\theta(\mathbf{f} | \bar{\boldsymbol{\omega}}, \bar{\mathbf{y}}, \bar{\mathbf{X}}) d\mathbf{f}$ using its analytical expression for the actual training data and then compute the likelihood of \mathbf{y} using Gauss-Hermite integration. Then we use Eq. 3 & 4 for learning the network parameters. At test time, to make full use of the training data, we combine the inducing inputs with the training data and use both to obtain the GP formulas and to make predictions. We note that with just using the inducing inputs at test time the model performs remarkably well, despite having almost no personalization component. See Appendix E.7 for a further discussion.

One issue that arises when using IPs in this manner is that they can distort the true class distribution and make the classifier more likely to predict a low-probability class. We address this issue by adjusting the output distribution. In general, let $p(y, \mathbf{x})$ and $q(y, \mathbf{x})$ be two distributions that differ only in the class probabilities, i.e. $p(\mathbf{x}|y) = q(\mathbf{x}|y)$, we get that the predictive distribution follows

$$\frac{q(y^* | \mathbf{x}^*)}{p(y^* | \mathbf{x}^*)} \propto \frac{q(\mathbf{x}^* | y^*) q(y^*)}{p(\mathbf{x}^* | y^*) p(y^*)} \implies q(y^* | \mathbf{x}^*) \propto \frac{q(y^*)}{p(y^*)} p(y^* | \mathbf{x}^*). \quad (5)$$

We use this to correct the GP predictions to the original class ratios at each tree node. We found in our experiments that this correction generally improves the classifier performance for unbalanced data.

4.3 Augmenting the model with inducing points: computational efficiency

Learning the full GP model described in Section 4.1 requires inverting a matrix of size N_c in the worst case (at the root node), which has $\mathcal{O}(N_c^3)$ run-time complexity and $\mathcal{O}(N_c^2)$ memory complexity. Therefore, we also propose an additional procedure for using the inducing points method to allow reduced complexity in low resource environments and scalability to larger data sizes per client.

This variant is based on the fully independent training conditional (FITC) method [65]. The key idea is to cast all the dependence on the inducing points and assume independence between the latent function values given the inducing points. Here for conciseness, we omit the subscripts denoting the client and the tree node. However, all quantities and data points are those that belong to a specific

client and tree node. Let $\bar{\mathbf{X}} \in \mathbb{R}^{M \times d}$ denote the pseudo-inputs (defined in the embedding space of the last layer of the NN), and $\bar{\mathbf{f}} \in \mathbb{R}^M$ the corresponding latent function values. Here as well, the inducing inputs are defined globally at the server level. We assume the following GP prior $p(\mathbf{f}, \bar{\mathbf{f}}) = \mathcal{N}\left(\mathbf{0}, \begin{bmatrix} \mathbf{K}_{NN} & \mathbf{K}_{NM} \\ \mathbf{K}_{MN} & \mathbf{K}_{MM} \end{bmatrix}\right)$, where \mathbf{K}_{MM} is the kernel between the inducing inputs, \mathbf{K}_{NN} is a diagonal matrix between the actual training data, \mathbf{K}_{NM} is the kernel between the data and the inducing inputs, and we placed a zero mean prior. The likelihood of the dataset when factoring the inducing variables and the Pólya-Gamma variables (one per training sample), and the posterior over \mathbf{f} , both have known analytical expressions. We can then obtain the posterior and marginal distributions by marginalizing over $\bar{\mathbf{f}}$. Here we will present the posterior and marginal distributions:

$$p(\mathbf{f} | \mathbf{X}, \mathbf{y}, \omega, \bar{\mathbf{X}}) = \mathcal{N}(\mathbf{f} | \mathbf{K}_{NM} \mathbf{B}^{-1} \mathbf{K}_{MN} \Lambda^{-1} \Omega^{-1} \kappa, \mathbf{K}_{NN} - \mathbf{K}_{NM} (\mathbf{K}_{MM}^{-1} - \mathbf{B}^{-1}) \mathbf{K}_{MN}), \quad (6)$$

$$p(\mathbf{y} | \mathbf{X}, \omega, \bar{\mathbf{X}}) \propto \mathcal{N}(\Omega^{-1} \kappa | \mathbf{0}, \Lambda + \mathbf{K}_{NM} \mathbf{K}_{MM}^{-1} \mathbf{K}_{MN}). \quad (7)$$

Where $\Omega = \text{diag}(\omega)$, $\kappa_j = y_j - 1/2$, $\Lambda = \Omega^{-1} + \text{diag}(\mathbf{K}_{NN} - \mathbf{K}_{NM} \mathbf{K}_{MM}^{-1} \mathbf{K}_{MN})$, and $\mathbf{B} = \mathbf{K}_{MM} + \mathbf{K}_{MN} \Lambda^{-1} \mathbf{K}_{NM}$. The important thing to note is that we only need to invert an $M \times M$ or a diagonal matrices. See full derivation in Appendix B. During test time, we use $\bar{\mathbf{f}}$ to get the posterior of f^* to compute the predictive posterior likelihood.

Now we can use the marginal or predictive distributions similarly to our proposal in Section 4.1 to learn the shared NN parameters. The complexity of applying this procedure is reduced to $\mathcal{O}(M^2 N_c + M^3)$ in run-time, and $\mathcal{O}(MN_c + M^2)$ in memory. While the (conditional) independence assumption between the latent function values may be restrictive, we found this method to be comparable with the full GP alternative in our experiments. Potentially, this can be attributed to the effect of sharing the inducing inputs among clients and the information that ω stores on \mathbf{f} .

5 Generalization bound

It is reasonable to expect that after we learned the system new clients will arrive. In such cases, we would like to use pFedGP without re-training the kernel function. Under this scenario, we can derive generalization bounds concerning only the GP classifier without taking into account the fixed neural network using PAC-Bayes bound [46]. Having meaningful guarantees can be very important in safety-critical applications. The PAC-Bayes bound for GPC [59] (with the Gibbs risk):

Theorem 1. *Given i.i.d. samples $D_c = \{(\mathbf{x}_i, y_i)\}_{i=1}^{N_c}$ of size N_c drawn from any data distribution over $\mathcal{X} \times \{-1, 1\}$, a GP posterior Q , and a GP prior P , the following bound holds, where the probability is over random data samples:*

$$Pr_{D_c}\{R(Q) > R_{D_c}(Q) + KL_{ber}^{-1}(R_{D_c}(Q), \epsilon(\delta, n, P, Q))\} \leq \delta. \quad (8)$$

Here, we have,

$$\begin{aligned} R(Q) &= \mathbb{E}_{(\mathbf{x}^*, y^*)}[Pr_{f^* \sim Q(f^* | \mathbf{x}^*, D_c)}\{\text{sign } f^* \neq y^*\}], \quad R_{D_c}(Q) = \frac{1}{N_c} \sum_{i=1}^{N_c} Pr_{f_i \sim Q(f_i | D_c)}\{\text{sign } f_i \neq y_i\} \\ \epsilon(\delta, N_c, P, Q) &= \frac{1}{N_c} \left(KL[Q || P] + \log \frac{N_c + 1}{\delta} \right), \quad KL_{ber}^{-1}(q, \epsilon) = \max_{p \in [0, 1]} KL_{ber}[q || p] \leq \epsilon \end{aligned} \quad (9)$$

An important observation in [59] is that the KL-divergence between the posterior and prior Gaussian processes is equivalent to the KL-divergence between the posterior and prior distribution of their values on the N_c training samples. While [59] assumed Q to be Gaussian, this observation still holds even without this assumption. However, when Q is no longer Gaussian, as is the case here, $KL[Q(\mathbf{f}) || P(\mathbf{f})]$ no longer has a closed-form expression. We can show that for the Pólya-Gamma augmentation:

$$\begin{aligned} KL[Q(\mathbf{f}) || P(\mathbf{f})] &= \mathbb{E}_{Q(\omega)}\{KL[Q(\mathbf{f} | \omega) || P(\mathbf{f})]\} - MI[\mathbf{f}; \omega] \\ &= \mathbb{E}_{Q(\omega)}\{KL[Q(\mathbf{f} | \omega) || P(\mathbf{f})]\} + \mathbb{E}_{Q(\mathbf{f}, \omega)}\left[\log \frac{Q(\omega)}{Q(\omega | \mathbf{f})}\right] \end{aligned} \quad (10)$$

where MI denotes the mutual information. Since $Q(\mathbf{f}|\omega)$ and $P(\mathbf{f})$ are Gaussian, the $KL[Q(\mathbf{f}|\omega)||P(\mathbf{f})]$ term has a close form expression so we only need to perform Monte-Carlo approximation on the expectation on ω on the first element. In the second expectation $Q(\omega)$ does not have a known expression. To estimate it, given $\{(\omega_i, \mathbf{f}_i)\}_{i=1}^N$ samples, we use $Q(\omega_i) \approx \frac{1}{N-1} \sum_{j \neq i} Q(\omega_i|\mathbf{f}_j)$. Note that if the summation for j includes \mathbf{f}_i , it might result in a biased estimator. Further details on estimating $KL[Q(\mathbf{f}) || P(\mathbf{f})]$ are in Appendix C.

To assess the quality of the bound, we partitioned the CIFAR-10 dataset to 100 clients. We trained a shared network using our full-GP variant on 90 clients and then recorded the generalization and test error on the remaining 10 clients four times, each with a different training set size. Figure 2 shows the estimation of the generalization error bound ($\delta = 0.01$) vs the actual error on the novel clients with the Gibbs classifier. First, we observe that indeed the bound is greater than the actual test error for all points and that it is not vacuous. There is a strong correlation between the actual error and the bound. Secondly, unlike worst-case bounds (e.g., VC-dimension), this bound depends on the actual data and not only the number of data points.

6 Experiments

We evaluated pFedGP against baseline methods on various learning setups. We present the result for the following model variants: (i) *pFedGP*, the full GP model (Section 4.1); (ii) *pFedGP-IP-data*, the model with IPs described in Section 4.2; and (iii) *pFedGP-IP-compute*, the model with IPs described in Section 4.3. For pFedGP and pFedGP-IP-compute, the results obtained by maximizing the predictive and marginal likelihood were similar, with a slight advantage to the former. Therefore, we present here the results only for the predictive alternative and defer the results of the marginal alternative to the Appendix. Additional experiments, ablation study and further analyses are provided in Appendix E. Unless stated otherwise, we report the average and the standard error of the mean (SEM) over three random seeds of the federate accuracy, defined as the average accuracy across all clients and samples.

Datasets. All methods were evaluated on CIFAR-10, CIFAR-100 [34], and CINIC-10 [13] datasets. CINIC-10 is more diverse since it combines images from CIFAR-10 and ImageNet [14].

Compared methods. We compared our method against the following baselines: (1) *Local*, pFedGP full model on each client with a private network and no collaboration with other clients; (2) *FedAvg* [47], a standard FL model with no personalization component; (3) *FOLA* [43], a Bayesian method that used a multivariate Gaussian product mechanism to aggregate local models; (4) *FedPer* [4], a PFL approach that learns a personal classifier for each client on top of a shared feature extractor; (5) *LG-FedAvg* [40], a PFL method that uses local feature extractor per client and global output layers; (6) *pFedMe* [67], a PFL method which adds a Moreau-envelopes loss term; (7) *FedU* [16], a recent multi-task learning approach for PFL that learns a model per client; (8) *pFedHN* [60], a recent PFL approach that uses a hypernetwork to generate client-specific networks.

Training protocol. We follow the training strategy proposed in [60]. We limit the training process to 1000 communication rounds, in each we sample five clients uniformly at random for model updates. The training procedure is different in the FOLA and pFedHN baselines, so we used an equivalent communication cost. In LG-FedAvg, we made an extra 200 communication rounds after a pre-training stage with the FedAvg model for 1000 communication rounds. In the local model, we performed 100 epochs of training for each client. In all experiments, we use a LeNet-based network [36] with two convolution and two fully connected layers. We tune the hyperparameters of all methods using a pre-allocated held-out validation set. Full experimental details are given in Appendix D.

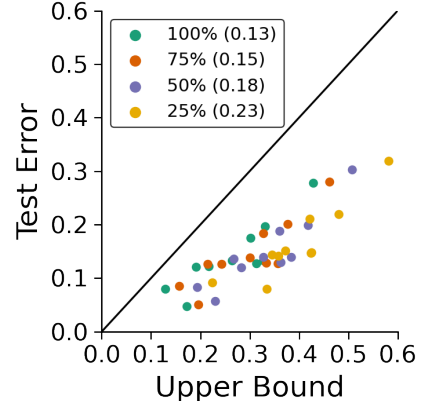


Figure 2: Test error vs an estimated upper bound over 10 clients with varying degrees of a training set data size. Each dot represents a combination of client and data size. In parenthesis - the average difference between the empirical and the test error.

Figure 2 shows the estimation of the generalization error bound ($\delta = 0.01$) vs the actual error on the novel clients with the Gibbs classifier. First, we observe that indeed the bound is greater than the actual test error for all points and that it is not vacuous. There is a strong correlation between the actual error and the bound. Secondly, unlike worst-case bounds (e.g., VC-dimension), this bound depends on the actual data and not only the number of data points.

Table 1: Test accuracy (\pm SEM) over 50, 100, 500 clients on CIFAR-10, CIFAR-100, and CINIC-10. The $\# \text{ samples}/\text{client}$ indicates the average number of training samples per client.

# clients	CIFAR-10			CIFAR-100			CINIC-10		
	50	100	500	50	100	500	50	100	500
	800	400	80	800	400	80	1800	900	180
Local	86.2 \pm 0.2	82.9 \pm 0.4	74.8 \pm 0.5	52.1 \pm 0.2	45.6 \pm 0.3	30.9 \pm 0.2	61.1 \pm 0.3	56.9 \pm 0.7	46.4 \pm 0.1
FedAvg [47]	56.4 \pm 0.5	59.7 \pm 0.5	54.0 \pm 0.5	23.6 \pm 0.2	24.0 \pm 0.2	20.4 \pm 0.0	45.6 \pm 0.4	44.7 \pm 0.5	45.7 \pm 0.5
FOLA [43]	55.9 \pm 3.3	52.1 \pm 3.1	45.9 \pm 0.3	25.5 \pm 1.5	22.4 \pm 1.3	18.7 \pm 0.1	45.2 \pm 0.3	43.4 \pm 0.3	38.3 \pm 0.2
FedPer [4]	83.8 \pm 0.8	81.5 \pm 0.5	76.8 \pm 1.2	48.3 \pm 0.6	43.6 \pm 0.2	25.6 \pm 0.3	70.6 \pm 0.2	68.4 \pm 0.5	62.2 \pm .05
LG-FedAvg [40]	87.9 \pm 0.3	83.6 \pm 0.7	64.7 \pm 0.7	43.6 \pm 0.2	37.5 \pm 0.9	20.3 \pm 0.5	59.5 \pm 1.1	59.9 \pm 2.1	52.5 \pm 0.8
pFedMe [67]	86.4 \pm 0.8	85.0 \pm 0.3	80.3 \pm 0.5	49.8 \pm 0.5	47.7 \pm 0.4	32.5 \pm 0.8	69.9 \pm 0.5	68.9 \pm 0.7	58.8 \pm 0.1
FedU [16]	80.6 \pm 0.3	78.1 \pm 0.5	65.6 \pm 0.4	41.1 \pm 0.2	36.0 \pm 0.2	15.9 \pm 0.4	59.3 \pm 0.2	55.4 \pm 0.6	41.6 \pm 0.5
pFedHN [60]	90.2 \pm 0.6	87.4 \pm 0.2	83.2 \pm 0.8	60.0 \pm 1.0	52.3 \pm 0.5	34.1 \pm 0.1	70.4 \pm 0.4	69.4 \pm 0.5	64.2 \pm .05
Ours									
pFedGP-IP-data	88.6 \pm 0.2	87.4 \pm 0.2	86.9 \pm 0.7	60.2 \pm 0.3	58.5 \pm 0.3	55.7 \pm 0.4	69.8 \pm 0.2	68.3 \pm 0.6	67.6 \pm 0.3
pFedGP-IP-compute	89.9 \pm 0.6	88.8 \pm 0.1	86.8 \pm 0.4	61.2 \pm 0.4	59.8 \pm 0.3	49.2 \pm 0.3	72.0 \pm 0.3	71.5 \pm 0.5	68.2 \pm 0.2
pFedGP	89.2 \pm 0.3	88.8 \pm 0.2	87.6 \pm 0.4	63.3 \pm 0.1	61.3 \pm 0.2	50.6 \pm 0.2	71.8 \pm 0.3	71.3 \pm 0.4	68.1 \pm 0.3

6.1 Personalization through class probabilities

We evaluated all methods using a standard PFL benchmark [60, 67]. We varied the total number of clients in the system from 50 to 500 and we set the number of classes per client to two/ten/four for CIFAR-10/CIFAR-100/CINIC-10 respectively. Since the total number of samples was kept fixed, the number of samples per client changed accordingly.

The results are presented in Table 1. They show that: (1) The performance of the *local* baseline is significantly impaired when the number of samples per client decreases, emphasizing the importance of federated learning in the presence of limited local data. (2) FedAvg and FOLA, which do not use personalized FL, perform poorly in this heterogeneous setup. (3) pFedGP outperforms or is on par with previous state-of-the-art approaches when local data is sufficient (e.g., 50 clients on all datasets). When the data size per node becomes limited, pFedGP achieves significant improvements over competing methods; note the 9% and 21% difference in CIFAR-100 over 100 and 500 clients, respectively. (4) pFedGP-IP-compute often achieves comparable results to pFedGP. (5) pFedGP-IP-data is especially helpful when few samples per class are available, e.g., CIFAR-100 with 500 clients. That last point is further illustrated by decoupling the effect of the *number of clients* from that of the *training set size*. To illustrate that, in Appendix E.2 we fixed the number of clients and varied the number of training samples per class. From this experiment, we deduced that both factors (individually) contribute to pFedGP success.

A desired property from PFL classifiers is the ability to provide uncertainty estimation. For example, in decision support systems, such as in healthcare applications, the decision-maker should have an accurate estimation of the classifier confidence in the prediction. Here, we quantify the uncertainty through calibration. Figure 3 compares all methods both visually and using common metrics [7, 23, 51] on the CIFAR-100 dataset with 50 clients. Expected calibration error (ECE) measures the weighted average between the classifier confidence and accuracy. Maximum calibration error (MCE) takes the maximum instead of the average. And, Brier score (BRI) [7] measures the average squared error between the labels and the prediction probabilities. The figure shows that pFedGP classifiers are best calibrated across all metrics in almost all cases. We note that with temperature scaling, the calibration of the baseline methods can be improved [23]; however, choosing the right temperature requires optimization over a separate validation set, which our model does not need. Additional calibration results, including temperature scaling, are presented in Appendix E.8.

Table 2: Test accuracy (\pm SEM) over 100 clients on noisy CIFAR-100. We also provide the relative accuracy decrease (%) w.r.t. the performance on the original CIFAR-100 data (see Table 1).

Method	Accuracy	Decrease (%)
FedPer [4]	28.1 \pm 0.9	-35.6
LG-FedAvg [40]	26.9 \pm 0.9	-28.3
pFedme [67]	33.2 \pm 0.6	-30.4
FedU [16]	35.0 \pm 0.2	-2.8
pFedHN [60]	38.9 \pm 0.5	-25.7
Ours		
pFedGP-IP-data	45.0 \pm 0.3	-23.1
pFedGP-IP-compute	47.1 \pm .05	-21.2
pFedGP	49.5 \pm 0.1	-19.2

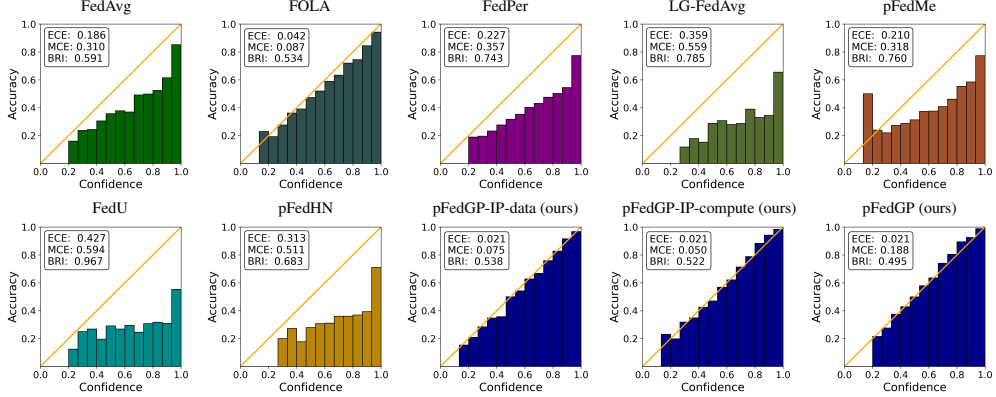


Figure 3: Reliability diagrams on CIFAR-100 with 50 clients. Each plot shows the expected & maximum calibration error (ECE & MCE) and the Brier Score (BRI). Lower is better. Diagonal indicates perfect calibration.

6.2 PFL with input noise

In real-world federated systems, the clients may employ different measurement devices for data collection (cameras, sensors, etc.), resulting in different input noise characteristics per client. Here, we investigate pFedGP performance in this type of personalization. To simulate that, we partitioned CIFAR-10/100 to 100 clients similarly to the protocol described in Section 6.1, we defined 57 unique distributions of image corruption noise [26] and we assigned a noise model to each client. Then for each example in each client we sampled a corruption noise according to the noise model allocated to that client. Here we show the results for the noisy CIFAR-100 dataset in Table 2. Further details on the perturbations performed and result for the noisy CIFAR-10 are given in the Appendix³. We observe a significant gap in favor of the pFedGP variants compared to baseline methods. Note that using global inducing points is slightly less beneficial in this case since they are defined globally and therefore are not tied to a specific noise type as the real client data is.

6.3 Generalization to out-of-distribution (OOD) novel clients

FL are dynamic systems. For example, novel clients may enter the system after the model was trained, possibly with a data distribution shift. Adapting to a new OOD client is both challenging and important for real-world FL systems. To evaluate pFedGP in this scenario, we followed the learning protocol proposed in [60]. We partitioned the CIFAR-10 dataset into two groups. The data in the first group was distributed between 90 clients for model training. The remaining data from the second group was distributed between an additional 10 clients that were excluded during training. Within each group, we set the class probabilities in each client by sampling from a Dirichlet distribution with the same α parameter. For the training group, we set $\alpha = 0.1$, trained the shared model using these clients, and froze it. Then, we evaluated the models on the second group by varying $\alpha \in \{.1, .25, .5, .75, 1\}$, on the remaining 10 clients. As α moves away from 0.1 the distribution shift between the two groups increases, resulting in more challenging OOD clients. Figure 4 reports the generalization gap as a function of the Dirichlet parameter α . The generalization gap is computed by taking the difference between the average test accuracy on the (ten) novel clients and the average test accuracy on the (ninety) clients used for training. From the figure,

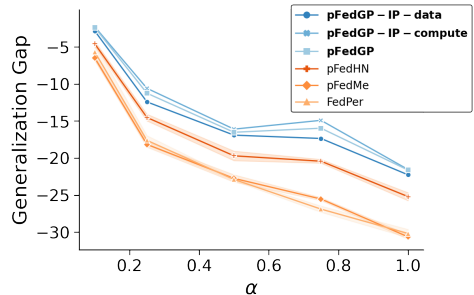


Figure 4: Generalization to novel clients on CIFAR-10.

³The noisy CIFAR-10 dataset is available at: [Noisy-CIFAR-10](#)

The noisy CIFAR-100 dataset is available at: [Noisy-CIFAR-100](#)

here as well, pFedGP achieves the best generalization performance for all values of α . Moreover, unlike baseline methods, pFedGP does not require *any* parameter tuning. Several baselines were excluded from the figure since they had a large generalization gap.

7 Conclusion

In this study, we proposed pFedGP, a novel method for PFL. pFedGP learns a kernel function, parameterized by a NN, that is shared between all clients using a personal GP classifier on each client. We proposed three variants for pFedGP, a full model approach that generally shows high performance and two extensions to it. The first is most beneficial when datasets are small while the second allows controlling the computational requirements of the model. We also derived PAC-Bayes generalization bound on novel clients and empirically showed that it gives non-vacuous guarantees. pFedGP provides well-calibrated predictions, generalizes well to OOD novel clients, and consistently outperforms competing methods.

Acknowledgements

This study was funded by a grant to GC from the Israel Science Foundation (ISF 737/2018), and by an equipment grant to GC and Bar-Ilan University from the Israel Science Foundation (ISF 2332/18). IA was funded by a grant from the Israeli innovation authority, through the AVATAR consortium.

References

- [1] Sawsan Abdulrahman, Hanine Tout, Hakima Ould-Slimane, Azzam Mourad, Chamseddine Talhi, and Mohsen Guizani. A survey on federated learning: The journey from centralized to distributed on-site learning and beyond. *IEEE Internet of Things Journal*, 8(7):5476–5497, 2021.
- [2] Idan Achituv, Aviv Navon, Yochai Yemini, Gal Chechik, and Ethan Fetaya. GP-Tree: A Gaussian process classifier for few-shot incremental learning. In *International Conference on Machine Learning*. PMLR, 2021.
- [3] Naman Agarwal, Ananda Theertha Suresh, Felix Xinnan X Yu, Sanjiv Kumar, and Brendan McMahan. cpSGD: Communication-efficient and differentially-private distributed SGD. In *Advances in Neural Information Processing Systems*, pages 7564–7575, 2018.
- [4] Manoj Ghuhan Arivazhagan, Vinay Aggarwal, Aaditya Kumar Singh, and Sunav Choudhary. Federated learning with personalization layers. *arXiv preprint arXiv:1912.00818*, 2019.
- [5] David Arthur and Sergei Vassilvitskii. k-means++ the advantages of careful seeding. In *Proceedings of the eighteenth annual ACM-SIAM symposium on Discrete algorithms*, pages 1027–1035, 2007.
- [6] Harkirat Singh Behl, Atilim Güneş Baydin, and Philip HS Torr. Alpha MAML: Adaptive model-agnostic meta-learning. *arXiv preprint arXiv:1905.07435*, 2019.
- [7] Glenn W Brier. Verification of forecasts expressed in terms of probability. *Monthly weather review*, 78(1):1–3, 1950.
- [8] Thang D Bui, Cuong V Nguyen, Siddharth Swaroop, and Richard E Turner. Partitioned variational inference: A unified framework encompassing federated and continual learning. *arXiv preprint arXiv:1811.11206*, 2018.
- [9] Roberto Calandra, Jan Peters, Carl Edward Rasmussen, and Marc Peter Deisenroth. Manifold Gaussian processes for regression. In *2016 International Joint Conference on Neural Networks (IJCNN)*, pages 3338–3345. IEEE, 2016.
- [10] Shuxiao Chen, Qingqing Zheng, Qi Long, and Weijie J Su. A theorem of the alternative for personalized federated learning. *arXiv preprint arXiv:2103.01901*, 2021.
- [11] Luca Corinzia, Ami Beuret, and Joachim M Buhmann. Variational federated multi-task learning. *arXiv preprint arXiv:1906.06268*, 2019.
- [12] Xinyan Dai, Xiao Yan, Kaiwen Zhou, Han Yang, Kelvin KW Ng, James Cheng, and Yu Fan. Hyper-sphere quantization: Communication-efficient SGD for federated learning. *arXiv preprint arXiv:1911.04655*, 2019.

- [13] Luke N Darlow, Elliot J Crowley, Antreas Antoniou, and Amos J Storkey. CINIC-10 is not Imagenet or CIFAR-10. *arXiv preprint arXiv:1810.03505*, 2018.
- [14] Jia Deng, Wei Dong, Richard Socher, Li-Jia Li, Kai Li, and Li Fei-Fei. Imagenet: A large-scale hierarchical image database. In *2009 IEEE conference on computer vision and pattern recognition*, pages 248–255. Ieee, 2009.
- [15] Yuyang Deng, Mohammad Mahdi Kamani, and Mehrdad Mahdavi. Adaptive personalized federated learning. *arXiv preprint arXiv:2003.13461*, 2020.
- [16] Canh T Dinh, Tung T Vu, Nguyen H Tran, Minh N Dao, and Hongyu Zhang. FedU: A unified framework for federated multi-task learning with Laplacian regularization. *arXiv preprint arXiv:2102.07148*, 2021.
- [17] Randal Douc, Eric Moulines, and David Stoffer. *Nonlinear time series: Theory, methods and applications with R examples*. CRC press, 2014.
- [18] John C Duchi, Michael I Jordan, and Martin J Wainwright. Privacy aware learning. *Journal of the ACM (JACM)*, 61(6):1–57, 2014.
- [19] Alireza Fallah, Aryan Mokhtari, and A. Ozdaglar. Personalized federated learning: A meta-learning approach. *Advances in Neural Information Processing Systems*, 2020.
- [20] Alireza Fallah, Aryan Mokhtari, and Asuman Ozdaglar. On the convergence theory of gradient-based model-agnostic meta-learning algorithms. In *International Conference on Artificial Intelligence and Statistics*, pages 1082–1092. PMLR, 2020.
- [21] Théo Galy-Fajou, Florian Wenzel, Christian Donner, and Manfred Opper. Multi-class Gaussian process classification made conjugate: Efficient inference via data augmentation. In *Uncertainty in Artificial Intelligence*, pages 755–765. PMLR, 2020.
- [22] Théo Galy-Fajou, Florian Wenzel, and Manfred Opper. Automated augmented conjugate inference for non-conjugate gaussian process models. In *International Conference on Artificial Intelligence and Statistics*, pages 3025–3035. PMLR, 2020.
- [23] Chuan Guo, Geoff Pleiss, Yu Sun, and Kilian Q Weinberger. On calibration of modern neural networks. In *International Conference on Machine Learning*, pages 1321–1330. PMLR, 2017.
- [24] Farzin Haddadpour and Mehrdad Mahdavi. On the convergence of local descent methods in federated learning. *arXiv preprint arXiv:1910.14425*, 2019.
- [25] Filip Hanzely and Peter Richtárik. Federated learning of a mixture of global and local models. *arXiv preprint arXiv:2002.05516*, 2020.
- [26] Dan Hendrycks and Thomas Dietterich. Benchmarking neural network robustness to common corruptions and perturbations. In *International Conference on Learning Representations*, 2019.
- [27] James Hensman, Alexander Matthews, and Zoubin Ghahramani. Scalable variational Gaussian process classification. In *Artificial Intelligence and Statistics*, pages 351–360. PMLR, 2015.
- [28] T. H. Hsu, Hang Qi, and M. Brown. Measuring the effects of non-identical data distribution for federated visual classification. *ArXiv*, abs/1909.06335, 2019.
- [29] Yutao Huang, Lingyang Chu, Zirui Zhou, Lanjun Wang, Jiangchuan Liu, Jian Pei, and Yong Zhang. Personalized cross-silo federated learning on non-IID data. In *Proceedings of the AAAI Conference on Artificial Intelligence*, 2021.
- [30] Peter Kairouz, H Brendan McMahan, Brendan Avent, Aurélien Bellet, Mehdi Bennis, Arjun Nitin Bhagoji, Keith Bonawitz, Zachary Charles, Graham Cormode, Rachel Cummings, et al. Advances and open problems in federated learning. *arXiv preprint arXiv:1912.04977*, 2019.
- [31] Sai Praneeth Karimireddy, Satyen Kale, Mehryar Mohri, Sashank Reddi, Sebastian Stich, and Ananda Theertha Suresh. SCAFFOLD: Stochastic controlled averaging for federated learning. In *International Conference on Machine Learning*, pages 5132–5143. PMLR, 2020.
- [32] Rahif Kassab and Osvaldo Simeone. Federated generalized Bayesian learning via distributed Stein variational gradient descent. *arXiv preprint arXiv:2009.06419*, 2020.
- [33] Jakub Konečný, H Brendan McMahan, Daniel Ramage, and Peter Richtárik. Federated optimization: Distributed machine learning for on-device intelligence. *arXiv preprint arXiv:1610.02527*, 2016.

[34] Alex Krizhevsky, Geoffrey Hinton, et al. Learning multiple layers of features from tiny images. Technical report, University of Toronto, 2009.

[35] V. Kulkarni, Milind Kulkarni, and A. Pant. Survey of personalization techniques for federated learning. *2020 Fourth World Conference on Smart Trends in Systems, Security and Sustainability (WorldS4)*, pages 794–797, 2020.

[36] Yann LeCun, Léon Bottou, Yoshua Bengio, and Patrick Haffner. Gradient-based learning applied to document recognition. *Proceedings of the IEEE*, 86(11):2278–2324, 1998.

[37] Tian Li, Anit Kumar Sahu, Mazyar Sanjabi, Manzil Zaheer, Ameet Talwalkar, and Virginia Smith. On the convergence of federated optimization in heterogeneous networks. *arXiv preprint arXiv:1812.06127*, 2018.

[38] Tian Li, Anit Kumar Sahu, Ameet Talwalkar, and Virginia Smith. Federated learning: Challenges, methods, and future directions. *IEEE Signal Processing Magazine*, 37(3):50–60, 2020.

[39] Zhenguo Li, Fengwei Zhou, Fei Chen, and Hang Li. Meta-SGD: Learning to learn quickly for few-shot learning. *arXiv preprint arXiv:1707.09835*, 2017.

[40] Paul Pu Liang, Terrance Liu, Liu Ziyin, Nicholas B Allen, Randy P Auerbach, David Brent, Ruslan Salakhutdinov, and Louis-Philippe Morency. Think locally, act globally: Federated learning with local and global representations. *arXiv preprint arXiv:2001.01523*, 2020.

[41] Tao Lin, Sebastian U Stich, Kumar Kshitij Patel, and Martin Jaggi. Don’t use large mini-batches, use local SGD. In *International Conference on Learning Representations*, 2019.

[42] Scott W Linderman, Matthew J Johnson, and Ryan P Adams. Dependent multinomial models made easy: stick breaking with the Pólya-Gamma augmentation. In *Proceedings of the 28th International Conference on Neural Information Processing Systems*, pages 3456–3464, 2015.

[43] Liangxi Liu and Feng Zheng. A Bayesian federated learning framework with multivariate gaussian product. *arXiv preprint arXiv:2102.01936*, 2021.

[44] Wesley Maddox, Shuai Tang, Pablo Moreno, Andrew Gordon Wilson, and Andreas Damianou. Fast adaptation with linearized neural networks. In *International Conference on Artificial Intelligence and Statistics*, pages 2737–2745. PMLR, 2021.

[45] Y. Mansour, M. Mohri, J. Ro, and A. T. Suresh. Three approaches for personalization with applications to federated learning. *ArXiv*, abs/2002.10619, 2020.

[46] David A McAllester. PAC-Bayesian stochastic model selection. *Machine Learning*, 51(1):5–21, 2003.

[47] Brendan McMahan, Eider Moore, Daniel Ramage, Seth Hampson, and Blaise Aguera y Arcas. Communication-efficient learning of deep networks from decentralized data. In *Artificial Intelligence and Statistics*, pages 1273–1282. PMLR, 2017.

[48] H Brendan McMahan, Daniel Ramage, Kunal Talwar, and Li Zhang. Learning differentially private recurrent language models. In *International Conference on Learning Representations*, 2018.

[49] Thomas Peter Minka. *A family of algorithms for approximate Bayesian inference*. PhD thesis, Massachusetts Institute of Technology, 2001.

[50] Viraaj Mothukuri, Reza M Parizi, Seyedamin Pouriyeh, Yan Huang, Ali Dehghantanha, and Gautam Srivastava. A survey on security and privacy of federated learning. *Future Generation Computer Systems*, 115:619–640, 2021.

[51] Mahdi Pakdaman Naeini, Gregory Cooper, and Milos Hauskrecht. Obtaining well calibrated probabilities using Bayesian binning. In *Proceedings of the AAAI Conference on Artificial Intelligence*, volume 29, 2015.

[52] Sebastian W. Ober, Carl E. Rasmussen, and Mark van der Wilk. The promises and pitfalls of deep kernel learning. *CoRR*, 2021.

[53] Nicholas G. Polson, James G. Scott, and Jesse Windle. Bayesian inference for logistic models using Pólya–Gamma latent variables. *Journal of the American Statistical Association*, pages 1339–1349, 2013.

[54] Joaquin Quinonero-Candela and Carl Edward Rasmussen. A unifying view of sparse approximate Gaussian process regression. *The Journal of Machine Learning Research*, 6:1939–1959, 2005.

[55] Carl Edward Rasmussen and Christopher K. I. Williams. *Gaussian Processes for Machine Learning*. The MIT Press, 2006.

[56] David Reeb, Andreas Doerr, Sebastian Gerwinn, and Barbara Rakitsch. Learning Gaussian processes by minimizing PAC-Bayesian generalization bounds. In *Proceedings of the 32nd International Conference on Neural Information Processing Systems*, pages 3341–3351, 2018.

[57] Amirhossein Reisizadeh, Aryan Mokhtari, Hamed Hassani, Ali Jadbabaie, and Ramtin Pedarsani. FedPAQ: A communication-efficient federated learning method with periodic averaging and quantization. In *International Conference on Artificial Intelligence and Statistics*, pages 2021–2031. PMLR, 2020.

[58] Ryan Rifkin and Aldebaro Klautau. In defense of one-vs-all classification. *The Journal of Machine Learning Research*, 5:101–141, 2004.

[59] Matthias Seeger. PAC-Bayesian generalisation error bounds for Gaussian process classification. *Journal of machine learning research*, 3(Oct):233–269, 2002.

[60] Aviv Shamsian, Aviv Navon, Ethan Fetaya, and Gal Chechik. Personalized federated learning using hypernetworks. In *International Conference on Machine Learning*. PMLR, 2021.

[61] Reza Shokri and Vitaly Shmatikov. Privacy-preserving deep learning. In *Proceedings of the 22nd ACM SIGSAC conference on computer and communications security*, pages 1310–1321, 2015.

[62] Virginia Smith, Chao-Kai Chiang, Maziar Sanjabi, and Ameet Talwalkar. Federated multi-task learning. In *Proceedings of the 31st International Conference on Neural Information Processing Systems*, pages 4427–4437, 2017.

[63] Jake Snell, Kevin Swersky, and Richard Zemel. Prototypical networks for few-shot learning. In *Proceedings of the 31st International Conference on Neural Information Processing Systems*, pages 4080–4090, 2017.

[64] Jake Snell and Richard Zemel. Bayesian few-shot classification with one-vs-each Pólya-Gamma augmented Gaussian processes. In *International Conference on Learning Representations*, 2021.

[65] Edward Snelson and Zoubin Ghahramani. Sparse Gaussian processes using pseudo-inputs. In *Advances in Neural Information Processing Systems*, pages 1257–1264. MIT Press, 2006.

[66] Sebastian U Stich. Local SGD converges fast and communicates little. In *International Conference on Learning Representations*, 2018.

[67] Canh T Dinh, Nguyen Tran, and Tuan Dung Nguyen. Personalized federated learning with Moreau envelopes. *Advances in Neural Information Processing Systems*, 33, 2020.

[68] Alysa Ziying Tan, Han Yu, Lizhen Cui, and Qiang Yang. Towards personalized federated learning. *arXiv preprint arXiv:2103.00710*, 2021.

[69] Minxue Tang, Xuefei Ning, Yitu Wang, Yu Wang, and Yiran Chen. Fedgp: Correlation-based active client selection for heterogeneous federated learning. *arXiv preprint arXiv:2103.13822*, 2021.

[70] Carlos Villacampa-Calvo, Bryan Zaldívar, Eduardo C Garrido-Merchán, and Daniel Hernández-Lobato. Multi-class Gaussian process classification with noisy inputs. *Journal of Machine Learning Research*, 22(36):1–52, 2021.

[71] Hongyi Wang, Mikhail Yurochkin, Yuekai Sun, Dimitris Papailiopoulos, and Yasaman Khazaei. Federated learning with matched averaging. In *International Conference on Learning Representations*, 2019.

[72] Jianyu Wang and Gauri Joshi. Cooperative SGD: A unified framework for the design and analysis of communication-efficient SGD algorithms. In *ICML Workshop on Coding Theory for Machine Learning*, 2019.

[73] Florian Wenzel, Théo Galy-Fajou, Christian Donner, Marius Kloft, and Manfred Opper. Efficient Gaussian process classification using Pólya-Gamma data augmentation. In *The AAAI Conference on Artificial Intelligence*, pages 5417–5424. AAAI Press, 2019.

[74] Christopher KI Williams and David Barber. Bayesian classification with Gaussian processes. *IEEE Transactions on Pattern Analysis and Machine Intelligence*, 20(12):1342–1351, 1998.

- [75] Andrew Gordon Wilson, Zhiting Hu, Ruslan Salakhutdinov, and Eric P. Xing. Deep kernel learning. In *International Conference on Artificial Intelligence and Statistics (AISTATS)*, 2016.
- [76] Andrew Gordon Wilson, Zhiting Hu, Ruslan Salakhutdinov, and Eric P Xing. Stochastic variational deep kernel learning. In *Proceedings of the 30th International Conference on Neural Information Processing Systems*, pages 2594–2602, 2016.
- [77] Qiang Yang, Yang Liu, Tianjian Chen, and Yongxin Tong. Federated machine learning: Concept and applications. *ACM Transactions on Intelligent Systems and Technology (TIST)*, 10(2):1–19, 2019.
- [78] Feng Yin, Zhidi Lin, Qinglei Kong, Yue Xu, Deshi Li, Sergios Theodoridis, and Shuguang Robert Cui. FedLoc: Federated learning framework for data-driven cooperative localization and location data processing. *IEEE Open Journal of Signal Processing*, 1:187–215, 2020.
- [79] Mikhail Yurochkin, Mayank Agarwal, Soumya Ghosh, Kristjan Greenewald, Nghia Hoang, and Yasaman Khazaeni. Bayesian nonparametric federated learning of neural networks. In *International Conference on Machine Learning*, pages 7252–7261. PMLR, 2019.
- [80] Chen Zhang, Yu Xie, Hang Bai, Bin Yu, Weihong Li, and Yuan Gao. A survey on federated learning. *Knowledge-Based Systems*, 216:106775, 2021.
- [81] Michael Zhang, Karan Sapra, Sanja Fidler, Serena Yeung, and Jose M Alvarez. Personalized federated learning with first order model optimization. *arXiv preprint arXiv:2012.08565*, 2020.
- [82] Yue Zhao, Meng Li, Liangzhen Lai, Naveen Suda, Damon Civin, and Vikas Chandra. Federated learning with non-IID data. *arXiv preprint arXiv:1806.00582*, 2018.
- [83] Fan Zhou and Guojing Cong. On the convergence properties of a K-step averaging stochastic gradient descent algorithm for nonconvex optimization. In *Proceedings of the 27th International Joint Conference on Artificial Intelligence*, pages 3219–3227, 2018.
- [84] Pan Zhou, Xiaotong Yuan, Huan Xu, Shuicheng Yan, and Jiashi Feng. Efficient meta learning via minibatch proximal update. *Advances in Neural Information Processing Systems*, 32:1534–1544, 2019.
- [85] Wennan Zhu, Peter Kairouz, Brendan McMahan, Haicheng Sun, and Wei Li. Federated heavy hitters discovery with differential privacy. In *International Conference on Artificial Intelligence and Statistics*, pages 3837–3847. PMLR, 2020.

A Extended background

A.1 The Pólya-Gamma augmentation

A random variable ω has a Pólya-Gamma distribution if it can be written as an infinite sum of independent gamma random variables:

$$\omega \stackrel{D}{=} \frac{1}{2\pi^2} \sum_{k=1}^{\infty} \frac{g_k}{(k-1/2)^2 + c^2/(4\pi^2)}, \quad (11)$$

where $b > 0$, $c \in \mathbb{R}$, and $g_k \sim \text{Gamma}(b, 1)$.

This random variable was proposed in [53] as it has the following desired property - For $b > 0$ the following identity holds:

$$\frac{(e^f)^a}{(1+e^f)^b} = 2^{-b} e^{\kappa f} \mathbb{E}_{\omega} [e^{-\omega f^2/2}], \quad (12)$$

where $\kappa = a - b/2$, and ω has the Pólya-Gamma distribution, $\omega \sim PG(b, 0)$. In [53] the authors also devised an efficient sampling algorithms for Pólya-Gamma random variables.

Suppose we are given with latent function values $\mathbf{f} \in \mathbb{R}^N$ having a binary classification assignment $\mathbf{y} \in \{0, 1\}^N$. Let the prior over $\mathbf{f} \sim \mathcal{N}(\boldsymbol{\mu}, \mathbf{K})$. The likelihood can be written as,

$$p(\mathbf{y}|\mathbf{f}) = \prod_{j=1}^n \sigma(f_j)^{y_j} (1 - \sigma(f_j))^{1-y_j} = \prod_{j=1}^n \frac{(e^{f_j})^{y_j}}{1+e^{f_j}} = \mathbb{E}_{\omega} \left[2^{-bn} \exp \left(\sum_{j=1}^n \kappa_j f_j - \frac{\omega_j f_j^2}{2} \right) \right], \quad (13)$$

where $\sigma(\cdot)$ is the sigmoid function. Namely, we used Eq. 12 to augment the model with Pólya-Gamma variables (one per sample) such that the original likelihood is recovered when marginalizing them out.

Now, the augmented likelihood, $p(\mathbf{y}|\mathbf{f}, \omega)$, is proportional to a diagonal Gaussian and the posteriors in the augmented space have known expressions:

$$\begin{aligned} p(\mathbf{f}|\mathbf{y}, \omega) &= \mathcal{N}(\mathbf{f}|\boldsymbol{\Sigma}(\mathbf{K}^{-1}\boldsymbol{\mu} + \boldsymbol{\kappa}), \boldsymbol{\Sigma}), \\ p(\omega|\mathbf{y}, \mathbf{f}) &= PG(1, \mathbf{f}). \end{aligned} \quad (14)$$

Where $\kappa_j = y_j - 1/2$, $\boldsymbol{\Sigma} = (\mathbf{K}^{-1} + \boldsymbol{\Omega})^{-1}$, and $\boldsymbol{\Omega} = \text{diag}(\omega)$. We can now sample from $p(\mathbf{f}, \omega|\mathbf{y}, \mathbf{X})$ using block Gibbs sampling and get Monte-Carlo estimations of the marginal and predictive distributions.

A.2 GP-Tree

Our method builds upon the method presented in [2]. It was shown to scale well both with dataset size and the number of classes, outperforming other GPC methods on standard benchmarks. We provide here a summary of this method, termed GP-Tree. GP-Tree uses the Pólya-Gamma augmentation, which is designed for binary classification tasks, in a (binary) tree-structure hierarchical model for multi-class classification tasks. Given a training dataset $D = (\mathbf{X}, \mathbf{y})$ of features and corresponding labels from $\{1, \dots, T\}$ classes, D is partitioned recursively to two subsets, according to classes, at each tree level until reaching leaf nodes with data from only one class. More concretely, initially, feature vectors for all samples are obtained (using a NN), then a class prototype is generated by averaging the feature vectors belonging to the same class for all classes. Finally, a tree is formed using the divisive hierarchical clustering algorithm k-means++ [5] with $k = 2$ on the class prototypes. Partitioning the data in this manner is sensible since NNs tend to generate points that cluster around a single prototype for each class [63]. After building the tree, a GP model is assigned to each node to make a binary decision based on the data associated with that node. Let $f_v \sim \mathcal{GP}(m_v, k_v)$ be the GP associated with node v . We denote all the GPs in the tree with \mathcal{F} . The induced likelihood of a data point having the class t is given by the unique path P^t from the root to the leaf node corresponding to that class:

$$p(y = t|\mathcal{F}) = \prod_{v \in P^t} \sigma(f_v)^{y_v} (1 - \sigma(f_v))^{1-y_v}, \quad (15)$$

where $y_v = 1$ if the path goes left at v and zero otherwise. y_v can be viewed as the (local) node label assignment of the example. Since this likelihood factorizes over the nodes, we can look at the nodes separately. Therefore, in the following, we will omit the subscript v for brevity; however, all datum and quantities are those that belong to a specific node v .

In [2] two methods for applying GP inference were suggested: a variational inference (VI) approach and a Gibbs sampling procedure. The former is used when datasets are large by constructing a variational lower bound to learn the model parameters (e.g., the NN parameters), while the latter is used for Bayesian inference only when using a fixed model. Here we will focus on learning and inference with the Gibbs sampling procedure only (see main text for further details). To obtain the augmented marginal distribution and augmented predictive distribution for a novel point \mathbf{x}^* at each node, we can sample $\boldsymbol{\omega}$ (a vector for each node) and use the following rules:

$$\begin{aligned} p(\mathbf{y}|\boldsymbol{\omega}, \mathbf{X}) &= \int p(\mathbf{y}|\boldsymbol{\omega}, \mathbf{X}, \mathbf{f})p(\mathbf{f})d\mathbf{f} \\ &\propto \mathcal{N}(\boldsymbol{\Omega}^{-1}\boldsymbol{\kappa}|\mathbf{0}, \mathbf{K} + \boldsymbol{\Omega}^{-1}), \end{aligned} \quad (16)$$

$$\begin{aligned} p(f^*|\mathbf{x}^*, \mathbf{X}, \mathbf{y}, \boldsymbol{\omega}) &= \mathcal{N}(f^*|\mu^*, \Sigma^*), \\ \mu^* &= (\mathbf{k}^*)^T(\boldsymbol{\Omega}^{-1} + \mathbf{K})^{-1}\boldsymbol{\Omega}^{-1}\boldsymbol{\kappa}, \\ \Sigma^* &= k^{**} - (\mathbf{k}^*)^T(\boldsymbol{\Omega}^{-1} + \mathbf{K})^{-1}\mathbf{k}^*, \end{aligned} \quad (17)$$

$$p(y^*|\mathbf{x}^*, \mathbf{X}, \mathbf{y}, \boldsymbol{\omega}) = \int p(y^*|f^*)p(f^*|\mathbf{x}^*, \mathbf{X}, \mathbf{y}, \boldsymbol{\omega})df^*. \quad (18)$$

Where we assumed a zero mean prior, $k^{**} = k(\mathbf{x}^*, \mathbf{x}^*)$, $\mathbf{k}^*[i] = k(\mathbf{x}_i, \mathbf{x}^*)$, and $\mathbf{K}[i, j] = k(\mathbf{x}_i, \mathbf{x}_j)$. The integral in Eq. 18 is intractable, but can be computed numerically with 1D Gaussian-Hermite quadrature.

B pFedGP-IP-compute detailed derivation

Here we describe in more detail our pFedGP-IP-compute variant. The key idea behind this method is to cast all the dependence on the inducing points and assume independence between the latent function values given the inducing points. Since the inference problem factorizes over the clients and tree nodes, we may compute all quantities separately for each client and tree node and only afterward aggregate the results. Therefore, in the below, we omit the subscripts denoting the client and node; however, all quantities belong to a specific client and node. You may recall that $\bar{\mathbf{X}} \in \mathbb{R}^{M \times d}$ denote the pseudo-inputs, defined in the embedding space of the last layer of the NN and are shared by all clients, and $\bar{\mathbf{f}} \in \mathbb{R}^M$ are the corresponding latent function values. We assume the following GP prior $p(\mathbf{f}, \bar{\mathbf{f}}) = \mathcal{N}(\mathbf{0}, [\mathbf{K}_{NN} \ \mathbf{K}_{NM}; \ \mathbf{K}_{MN} \ \mathbf{K}_{MM}])$. The data likelihood of the dataset when factoring the inducing variables and the Pólya-Gamma variables (one per training sample) is proportional to a Gaussian:

$$p(\mathbf{y}|\mathbf{X}, \boldsymbol{\omega}, \bar{\mathbf{f}}, \bar{\mathbf{X}}) = \prod_{n=1}^N p(y_n|\mathbf{x}_n, \boldsymbol{\omega}, \bar{\mathbf{f}}, \bar{\mathbf{X}}) \propto \mathcal{N}(\boldsymbol{\Omega}^{-1}\boldsymbol{\kappa}|\mathbf{K}_{NM}\mathbf{K}_{MM}^{-1}\bar{\mathbf{f}}, \boldsymbol{\Lambda}), \quad (19)$$

where, $\boldsymbol{\Omega} = \text{diag}(\boldsymbol{\omega})$, $\kappa_j = y_j - 1/2$, and $\boldsymbol{\Lambda} = \boldsymbol{\Omega}^{-1} + \text{diag}(\mathbf{K}_{NN} - \mathbf{K}_{NM}\mathbf{K}_{MM}^{-1}\mathbf{K}_{MN})$.

The posterior over $\bar{\mathbf{f}}$ is obtained using Bayes rule:

$$p(\bar{\mathbf{f}}|\boldsymbol{\omega}, \mathbf{y}, \mathbf{X}, \bar{\mathbf{X}}) = \mathcal{N}(\bar{\mathbf{f}}|\mathbf{K}_{MM}\mathbf{B}^{-1}\mathbf{K}_{MN}\boldsymbol{\Lambda}^{-1}\boldsymbol{\Omega}^{-1}\boldsymbol{\kappa}, \mathbf{K}_{MM}\mathbf{B}^{-1}\mathbf{K}_{MM}), \quad (20)$$

where $\mathbf{B} = \mathbf{K}_{MM} + \mathbf{K}_{MN}\boldsymbol{\Lambda}^{-1}\mathbf{K}_{NM}$.

The posterior distribution over \mathbf{f} can be obtained by marginalization over $\bar{\mathbf{f}}$:

$$\begin{aligned} p(\mathbf{f}|\boldsymbol{\omega}, \mathbf{y}, \mathbf{X}, \bar{\mathbf{X}}) &= \int p(\mathbf{f}|\bar{\mathbf{f}}, \mathbf{X}, \bar{\mathbf{X}})p(\bar{\mathbf{f}}|\boldsymbol{\omega}, \mathbf{y}, \mathbf{X}, \bar{\mathbf{X}})d\bar{\mathbf{f}} \\ &= \mathcal{N}(\mathbf{f}|\mathbf{K}_{NM}\mathbf{B}^{-1}\mathbf{K}_{MN}\boldsymbol{\Lambda}^{-1}\boldsymbol{\Omega}^{-1}\boldsymbol{\kappa}, \mathbf{K}_{NN} - \mathbf{K}_{NM}(\mathbf{K}_{MM}^{-1} - \mathbf{B}^{-1})\mathbf{K}_{MN}). \end{aligned} \quad (21)$$

We note that while we use $\bar{\mathbf{f}}$ for predictions, we still need \mathbf{f} in order to sample $\boldsymbol{\omega}$.

Given ω and the expression for the posterior over $\bar{\mathbf{f}}$ we can compute the predictive distribution for a novel input \mathbf{x}^* :

$$\begin{aligned} p(f^* | \mathbf{x}^*, \omega, \mathbf{y}, \mathbf{X}, \bar{\mathbf{X}}) &= \int p(f^* | \mathbf{x}^*, \bar{\mathbf{f}}) p(\bar{\mathbf{f}} | \omega, \mathbf{y}, \mathbf{X}, \bar{\mathbf{X}}) d\bar{\mathbf{f}} \\ &= \mathcal{N}(f^* | (\mathbf{k}^*)^T \mathbf{B}^{-1} \mathbf{K}_{MN} \boldsymbol{\Lambda}^{-1} \boldsymbol{\Omega}^{-1} \boldsymbol{\kappa}, k^{**} - (\mathbf{k}^*)^T (\mathbf{K}_{MM}^{-1} - \mathbf{B}^{-1}) \mathbf{k}^*), \end{aligned} \quad (22)$$

where $k^{**} = k(\mathbf{x}^*, \mathbf{x}^*)$, and $\mathbf{k}^*[i] = k(\bar{\mathbf{x}}_i, \mathbf{x}^*)$.

The marginal distribution is given by:

$$p(\mathbf{y} | \omega, \mathbf{X}, \bar{\mathbf{X}}) = \int p(\mathbf{y} | \omega, \bar{\mathbf{f}}, \mathbf{X}, \bar{\mathbf{X}}) p(\bar{\mathbf{f}} | \bar{\mathbf{X}}) d\bar{\mathbf{f}} \propto \mathcal{N}(\boldsymbol{\Omega}^{-1} \boldsymbol{\kappa} | \mathbf{0}, \boldsymbol{\Lambda} + \mathbf{K}_{NM} \mathbf{K}_{MM}^{-1} \mathbf{K}_{MN}). \quad (23)$$

The full model marginal likelihood is given by:

$$\mathcal{L}_c^{ML}(\theta; D_c) = \sum_v \log p_\theta(\mathbf{y}_v | \mathbf{X}_v, \bar{\mathbf{X}}_v) = \sum_v \log \int p_\theta(\mathbf{y}_v | \omega_v, \mathbf{X}_v, \bar{\mathbf{X}}_v) p(\omega_v) d\omega_v, \quad (24)$$

and the predictive likelihood for a single data point \mathbf{x}^* having the class y^* :

$$\begin{aligned} \mathcal{L}_c^{PL}(\theta; \mathbf{x}^*, y^*) &= \sum_{v \in P^{y^*}} \log p_\theta(y_v^* | \mathbf{x}_v^*, \mathbf{y}_v, \mathbf{X}_v, \bar{\mathbf{X}}_v) \\ &= \sum_{v \in P^{y^*}} \log \int p_\theta(y_v^* | \omega_v, \mathbf{x}_v^*, \mathbf{y}_v, \mathbf{X}_v, \bar{\mathbf{X}}_v) p(\omega_v) d\omega_v. \\ &= \sum_{v \in P^{y^*}} \log \int p(\omega_v) \int p_\theta(y_v^* | f_v^*) p(f_v^* | \omega_v, \mathbf{x}_v^*, \mathbf{y}_v, \mathbf{X}_v, \bar{\mathbf{X}}_v) df_v^* d\omega_v. \end{aligned} \quad (25)$$

To learn the model parameters, we first use block gibbs sampling with the posterior distributions $p(\mathbf{f} | \mathbf{y}, \omega, \mathbf{X}, \bar{\mathbf{X}})$, and $p(\omega | \mathbf{y}, \mathbf{f}) = PG(\mathbf{1}, \mathbf{f})$. Then, we use Fisher's identity [17] to obtain gradients w.r.t the model parameters with the full model marginal or predictive likelihoods.

To speed up inference at test time, some computations that do not depend on \mathbf{x}^* can be done offline. Importantly, we can sample and cache ω and use it to compute $\boldsymbol{\Lambda}$ and the Cholesky decomposition of \mathbf{B} .

C Generalization bound - derivation

In Section 5 we presented an expression for the KL-divergence between the posterior and the prior (Eq. 10). Now we present the derivation:

$$\begin{aligned} KL[Q(\mathbf{f}) || P(\mathbf{f})] &= \int Q(\mathbf{f}) \log \frac{Q(\mathbf{f})}{P(\mathbf{f})} d\mathbf{f} \\ &= \int Q(\mathbf{f}, \omega) \log \frac{Q(\mathbf{f})}{P(\mathbf{f})} d\mathbf{f} d\omega \\ &= \int Q(\mathbf{f}, \omega) \log \frac{Q(\mathbf{f})Q(\omega | \mathbf{f})}{P(\mathbf{f})Q(\omega | \mathbf{f})} d\mathbf{f} d\omega \\ &= \int Q(\mathbf{f}, \omega) \log \frac{Q(\mathbf{f} | \omega)}{P(\mathbf{f})} d\mathbf{f} d\omega + \int Q(\mathbf{f}, \omega) \log \frac{Q(\omega)}{Q(\omega | \mathbf{f})} d\mathbf{f} d\omega \\ &= \int Q(\mathbf{f}, \omega) \log \frac{Q(\mathbf{f} | \omega)}{P(\mathbf{f})} d\mathbf{f} d\omega + \int Q(\mathbf{f}, \omega) \log \frac{Q(\mathbf{f})Q(\omega)}{Q(\mathbf{f}, \omega)} d\mathbf{f} d\omega \\ &= \mathbb{E}_{Q(\omega)} \{KL[Q(\mathbf{f} | \omega) || P(\mathbf{f})]\} - MI[\mathbf{f}; \omega], \end{aligned} \quad (26)$$

Where, the KL-divergence in the expectation term is between the prior, $P(\mathbf{f}) = \mathcal{N}(\boldsymbol{\mu}, \mathbf{K})$, and the posterior, $Q(\mathbf{f} | \omega) = \mathcal{N}(\boldsymbol{\Sigma}(\mathbf{K}^{-1} \boldsymbol{\mu} + \boldsymbol{\kappa}), \boldsymbol{\Sigma})$. Therefore, it has the following closed form:

$$KL[Q(\mathbf{f} | \omega) || P(\mathbf{f})] = \frac{1}{2} \{ \log \frac{|\mathbf{K}|}{|\boldsymbol{\Sigma}|} - N_c + \text{tr}(\mathbf{K}^{-1} \boldsymbol{\Sigma}) + (\boldsymbol{\Sigma}(\mathbf{K}^{-1} \boldsymbol{\mu} + \boldsymbol{\kappa}) - \boldsymbol{\mu})^T \mathbf{K}^{-1} (\boldsymbol{\Sigma}(\mathbf{K}^{-1} \boldsymbol{\mu} + \boldsymbol{\kappa}) - \boldsymbol{\mu}) \} \quad (27)$$

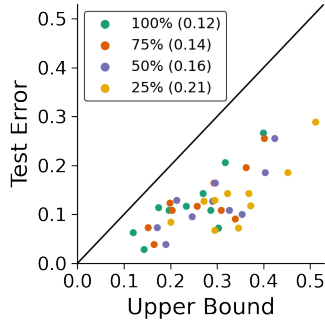


Figure 5: Test error vs. an estimated upper bound over 10 clients on CIFAR-10 with varying degrees of a training set data size using the Bayes classifier. Each dot represents a combination of client and data size. In parenthesis - average difference between the empirical and the test error.

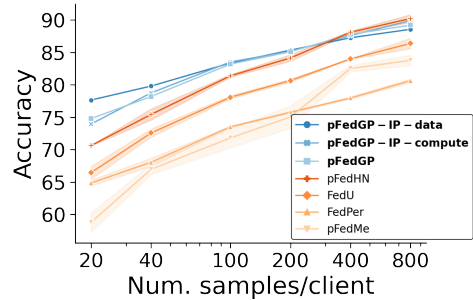


Figure 6: Model performance with varying degrees of average number of training samples per client (x-axis in log scale). Results are over 50 clients on CIFAR-10.

D Experimental details

Datasets. We evaluated pFedGP on the CIFAR-10, CIFAR-100 [34], and CINIC-10 [13] datasets. CIFAR-10/100 contain 60K images from 10/100 distinct classes, respectively, split to 50K for training and 10K for testing. CINIC-10 is a more diverse dataset. It is an extension of CIFAR-10 via the addition of down-sampled ImageNet [14] images. It contains 270K images split equally to train, validation, and test sets from 10 distinct classes.

Data assignment. For partitioning the data samples across clients we followed the procedure suggested in [60, 67]. This procedure produces clients with varying number of samples and a unique set of k classes for each client. First, we sampled k classes for each client. In general, we used $k = 2$ in CIFAR-10 experiments (e.g., Sections 5 & 6.1), $k = 10$ in CIFAR-100 experiments (e.g., Sections 6.1 & 6.2), and $k = 4$ in CINIC-10 experiments (e.g., Section 6.1). Next, to assign unique images for each client, we iterated over the classes and clients; for each client i having the class c , we sampled an unnormalized class fraction $\alpha_{i,c} \sim U(.4, .6)$. We then assigned to the i^{th} client $\frac{\alpha_{i,c}}{\sum_j \alpha_{j,c}}$ images from the overall samples of class c .

Hyperparameter tuning. We used a validation set for hyperparameter selection and early stopping in all methods. For the CIFAR datasets, we pre-allocated a validation set of size 10K from the training set. For the CINIC-10 dataset, we used the original split having a validation set of size 90K. The hyperparameters for all methods and all datasets were selected based on the learning setups with 50 clients. We searched over the learning-rates $\{1e-1, 5e-2, 1e-2, 5e-3\}$ for all methods, and personal learning-rates $\{5e-2, 1e-2, 5e-3, 1e-3\}$ for baseline methods only (pFedGP is a non-parametric approach and therefore does not optimize any private parameters). For pFedGP we searched over the number of epochs on sampled clients during training in $\{1, 3\}$, which is substantially less than baseline methods which usually use 20 epochs or more. We also searched over a scaling factor for the loss function in $\{1, 2\}$. We used the RBF kernel function with a fixed length scale of 1 and an output scale of 8. We used 20 parallel Gibbs chains for training and 30 parallel Gibbs chains for testing with 5 MCMC steps between samples in both. We note that as the number of steps increases usually the model becomes better calibrated, but without a discernible accuracy gain. In pFedGP-IP-data and pFedGP-IP-compute experiments, we used 100 inducing points per class. All experiments were done on NVIDIA GeForce RTX 2080 Ti having 11GB of memory.

Noisy datasets (Sections 6.2 & E.3). To generate a noisy version of the CIFAR-10 and CIFAR-100 datasets, we used the image-corruptions package [26]. We simulated the following 19 corruptions (Gaussian noise, shot noise, impulse noise, defocus blur, glass blur, motion blur, zoom blur, snow, frost, fog, brightness, contrast, elastic transform, pixelate, jpeg compression, speckle noise, Gaussian blur, spatter, saturate) with a corruption severity of (3, 4, 5), resulting in 57 unique noise models.

Table 3: Test accuracy (\pm SEM) over 100 clients on noisy CIFAR-10 under a homogeneous class distribution.

Method	Accuracy
FedAvg [47]	42.0 ± 0.2
FedPer [4]	38.2 ± 2.0
LG-FedAvg [40]	41.5 ± 0.2
pFedme [67]	36.3 ± 0.0
FedU [16]	24.8 ± 0.0
pFedHN [60]	35.7 ± 0.3
Ours	
pFedGP-IP-data	$46.1 \pm .05$
pFedGP-IP-compute	46.5 ± 0.5
pFedGP	46.7 ± 0.2

Table 4: Test accuracy (\pm SEM) over 50, 100 clients on CIFAR-10 under a homogeneous class distribution.

Method	# clients	
	50	100
FedAvg [47]	66.2 ± 0.3	64.6 ± 0.2
FedPer [4]	56.8 ± 0.1	50.9 ± 0.4
pFedMe [67]	46.9 ± 0.5	44.4 ± 0.3
FedU [16]	29.6 ± 0.6	26.3 ± 0.5
pFedHN [60]	62.8 ± 0.5	56.5 ± 0.1
Ours		
pFedGP-IP-data	62.7 ± 0.7	62.4 ± 0.5
pFedGP-IP-compute	65.8 ± 0.3	65.2 ± 0.4
pFedGP	66.2 ± 0.3	65.7 ± 0.2

E Additional experiments

E.1 Generalization bound with the Bayes risk

In Section 5 we assessed the quality of the lower bound with the Gibbs risk. However, often we are interested in a deterministic predictor. Also, we would like to get an estimate of the error with a classifier that is closer to our estimate of y^* with the Gauss-Hermite quadrature. This can be achieved with the Bayes risk [56] defined by $R_{Bayes}(Q) := \mathbb{E}_{(\mathbf{x}^*, y^*)}[\text{sign}(\mathbb{E}_{f^* \sim Q(f^* | \mathbf{x}^*, D_c)}[f^*]) \neq y^*]$. Figure 5 shows an estimation of the generalization error bound vs. the actual error on the novel clients with the Bayes classifier. From this figure we observe similar patterns to those seen in Figure 2. In general, the Bayes classifier performs better than the Gibbs classifier.

E.2 Varying the training set size

To decouple the effect of the local dataset size from the number of clients in the system, we altered the setting in Section 6.1. Here, we fixed the number of clients to 50 and used stratified sampling to sample $\{1000, 2000, 5000, 10000, 20000, 40000\}$ examples from the training dataset of CIFAR-10, where 40000 is the total number of training examples. Then, similar to Section 6.1 we randomly assigned two classes per client and partitioned the (sampled) data across clients. Figure 6 shows that all methods suffer from accuracy degradation when the training data size decrease; however, in pFedGP methods, the reduction is less severe compared to baseline methods. We especially note pFedGP-IP-data which shows remarkable accuracy in the extremely low data regime (77.7% accuracy with only 1000 training examples). These results can be attributed to the sharing of the inducing inputs which effectively increase the size of the training data per client. The LG-FedAvg baseline was excluded from this figure since it showed low accuracy.

E.3 PFL with input noise under a homogeneous class distribution

In Section 6.2 we evaluated pFedGP under two types of variations between the clients: (i) a unique input noise, and (ii) in the class distribution. It was done on the CIFAR-100 dataset with 100 clients. Here, we consider only a shift in the input noise between clients while having a balanced class distribution in all clients. We do so on the CIFAR-10 dataset (i.e., each client has 10 classes distributed approximately equal). Similarly to Section 6.2 we configured 100 clients, distributed the data among them, and assigned a noise model to each client from a closed-set of 57 noise distributions. Table 3 shows that in this setting as well, pFedGP and its variants achieve high accuracy and surpass all baseline methods by a large margin. From the table, we also notice that FedAvg, which performs well in balanced class distribution setups, outperforms all competing methods except ours.

Table 5: pFedGP model variants test accuracy (\pm SEM) over 50, 100, 500 clients on CIFAR-10, CIFAR-100, and CINIC-10. The $\# \text{ samples}/\text{client}$ indicates the average number of training samples per client.

# clients # samples/client	CIFAR-10			CIFAR-100			CINIC-10		
	50 800	100 400	500 80	50 800	100 400	500 80	50 1800	100 900	500 180
pFedGP-IP-data w/o personalization	88.6 \pm 1.0	87.0 \pm 0.2	86.4 \pm 0.7	58.1 \pm 0.3	57.4 \pm 0.6	55.4 \pm 0.2	69.2 \pm 0.3	68.2 \pm 0.9	67.9 \pm 0.1
pFedGP-IP-data	88.6 \pm 0.2	87.4 \pm 0.2	86.9 \pm 0.7	60.2 \pm 0.3	58.5 \pm 0.3	55.7 \pm 0.4	69.8 \pm 0.2	68.3 \pm 0.6	67.6 \pm 0.3
pFedGP-IP-compute-marginal	89.8 \pm 0.6	88.8 \pm 0.3	87.8 \pm 0.3	60.9 \pm 0.4	58.8 \pm 0.3	46.7 \pm 0.3	72.1 \pm 0.2	71.1 \pm 0.6	67.5 \pm 0.2
pFedGP-IP-compute-predictive	89.9 \pm 0.6	88.8 \pm 0.1	86.8 \pm 0.4	61.2 \pm 0.4	59.8 \pm 0.3	49.2 \pm 0.3	72.0 \pm 0.3	71.5 \pm 0.5	68.2 \pm 0.2
pFedGP-marginal	89.0 \pm 0.1	88.0 \pm 0.2	86.8 \pm 0.2	63.7 \pm 0.1	61.4 \pm 0.3	50.3 \pm 0.05	71.6 \pm 0.3	71.0 \pm 0.6	68.5 \pm 0.2
pFedGP-predictive	89.2 \pm 0.3	88.8 \pm 0.2	87.6 \pm 0.4	63.3 \pm 0.1	61.3 \pm 0.2	50.6 \pm 0.2	71.8 \pm 0.3	71.3 \pm 0.4	68.1 \pm 0.3

E.4 Homogeneous federated learning with CIFAR-10

pFedGP is a non-parametric classifier offered for personalized federated learning. Therefore, it only needs to model classes that are present in the training set. Here, for completeness, we evaluate pFedGP against top-performing baselines on the CIFAR-10 dataset, where all classes are represented in all clients. We do so on a homogeneous federated learning setup, i.e., all classes are distributed equally across all clients. Data assignment was done similarly to the procedure described in Section 6.1 (see Section D for more details). Table 4 shows that pFedGP outperforms all PFL baseline methods by a large margin in this setting as well. An interesting yet expected observation from the table is that FedAvg performs well under this (IID) setup. This result connects to a recent study that suggested that under a smooth, strongly convex loss when the data heterogeneity is below some threshold, FedAvg is minimax optimal [10]. We note here that modeling classes that are not present in the training set with pFedGP can be accomplished easily with one of the inducing points variants of pFedGP.

E.5 Computing demands

Table 6: pFedGP-IP-compute vs. pFedGP full model test accuracy and average predictive posterior inference run-time (\pm STD) as a function of the number of inducing points (IPs) over 50 clients on CINIC-10.

Num. IPs	80	160	240	320	400		Full GP
Accuracy (%)	70.2	71.0	71.4	71.5	71.5		71.3
Run time (sec.)	$0.15 \pm .02$	$0.21 \pm .03$	$0.27 \pm .04$	$0.34 \pm .05$	$0.42 \pm .06$		$1.08 \pm .16$

Here, we compare between pFedGP full model (Section 4.1) and pFedGP-IP-compute (Section 4.3) in terms of accuracy and run-time during prediction time. The key component controlling the computational demand of pFedGP during test time is the predictive likelihood (Equations 17 & 22). After the training phase, when a new test sample arrives, computing the predictive distributions can be done efficiently by using cached components that depend only on the training data (e.g., the Cholesky decomposition of \mathbf{B}) and can be calculated offline. Therefore, to quantify the impact of using pFedGP-IP-compute compared to the full GP model, we recorded in Table 6 the federated accuracy and average time per client for calculating the predictive distribution for all test examples as a function of the number of inducing points. The comparison was done on the pre-allocated test set from the CINIC-10 dataset over 50 clients (i.e., ~ 1800 test examples per client divided to 4 classes) using a model that was trained with 100 inducing points. The table shows a significant improvement in the run time compared to the full model without any (or only minor) accuracy degradation. We note here that including the network processing time will add a constant factor of 0.03 seconds.

E.6 Predictive vs marginal likelihood

In the main text, we presented two alternatives for learning the model parameters with pFedGP and pFedGP-IP-compute, the predictive likelihood and the marginal likelihood (see Section 4). We now compare between these two alternatives in Table 5 under the standard setup presented in Section 6.1. The table shows that for both pFedGP and pFedGP-IP-compute the two variants are comparable with

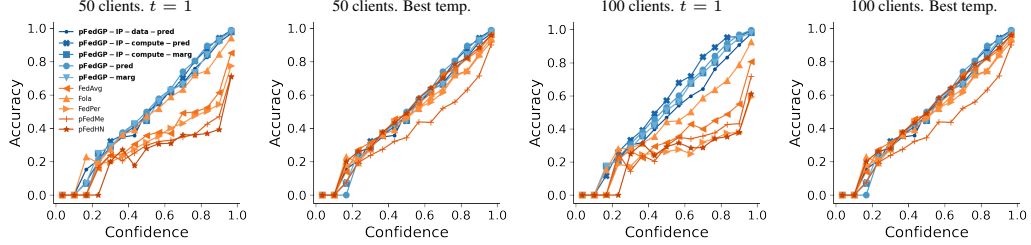


Figure 7: Reliability diagrams over 50, 100 clients on CIFAR-100.

a slight advantage to the predictive likelihood objective. Nevertheless, using the marginal likelihood usually results in a better calibrated model (Section E.8).

E.7 pFedGP-IP-data without (almost) any personalization

Recall that for the pFedGP-IP-data variant during training we build the kernel with the (shared) inducing inputs only. Yet, during test time, to account for the personal data, we use both the inducing inputs and the training data of the client for building the kernel. This method is especially effective in cases where the data per client is limited. Here, we evaluate this method without using the actual training data during test time. This means that the only personalization derives from the personal tree structure that is formed based on the actual training data of the client. Remarkably, Table 5 shows that using this strategy yields high accuracy as well and it is often comparable to pFedGP-IP-data.

E.8 Reliability diagrams

Now we present additional reliability diagrams for CIFAR-100 with 50 and 100 clients, with and without temperature scaling (See Figure 7 for unified diagrams and Figures 8 - 11 for separate diagrams). For each baseline we applied a grid search over a temperature $t \in \{0.1, 0.2, 0.5, 1.0, 2.0, 5.0, 10.0, 20.0, 50.0, 100.0, 200.0, 500.0, 1000.0\}$, chose the best temperature based on the pre-allocated validation set according to the ECE, and generated the diagram using the test set data. In addition, we present here reliability diagrams obtained by optimizing the marginal likelihood for pFedGP and pFedGP-IP-compute. From the figures, pFedGP does not gain from temperature scaling as baseline methods do since it is a calibrated classifier by design. Although this procedure improves the calibration of baseline methods, we note that finding the right temperature requires having a separate validation set which often can be challenging to obtain for problems in the low data regime.

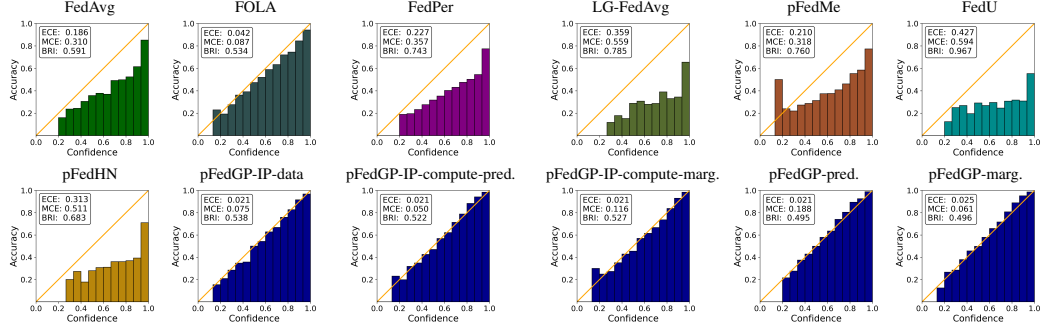


Figure 8: Reliability diagrams on CIFAR-100 with 50 clients. Default temperature ($t = 1$). The last 5 figures are ours.

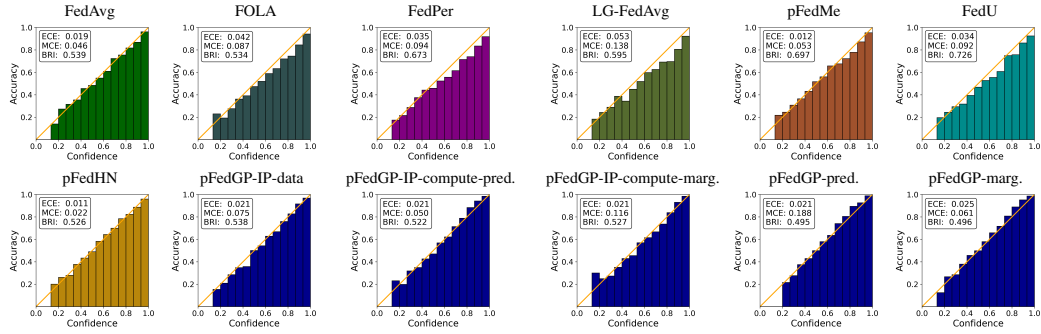


Figure 9: Reliability diagrams on CIFAR-100 with 50 clients. Best temperature. The last 5 figures are ours.

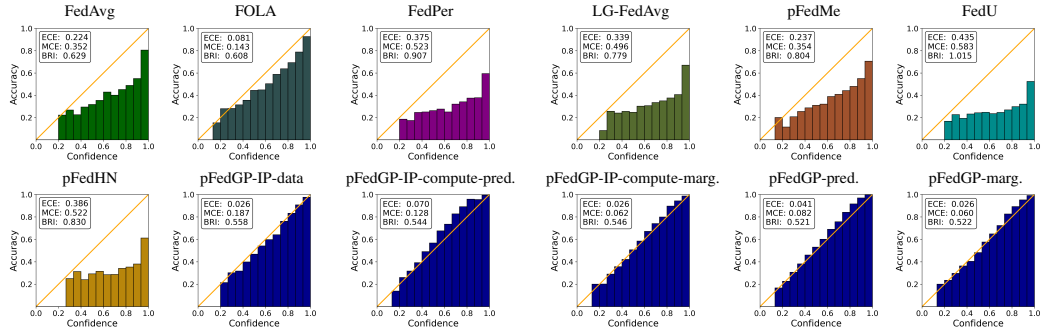


Figure 10: Reliability diagrams on CIFAR-100 with 100 clients. Default temperature ($t = 1$). The last 5 figures are ours.

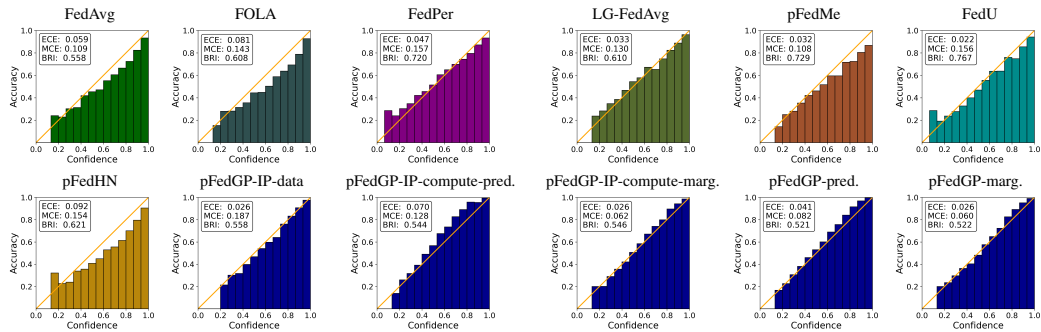


Figure 11: Reliability diagrams on CIFAR-100 with 100 clients. Best temperature. The last 5 figures are ours.